



OPEN

A novel risk score model of lactate metabolism for predicting outcomes and immune signatures in acute myeloid leukemia

Ze-min Huang^{1,2}, Jing Wei^{1,2}, Xiao-wen Pan^{1,2}, Xing-biao Chen^{1,2} & Zi-yuan Lu¹✉

Acute myeloid leukemia (AML) is a malignant tumor with high recurrence and refractory rates and low survival rates. Increased glycolysis is characteristic of metabolism in AML blast cells and is also associated with chemotherapy resistance. The purpose of this study was to use gene expression and clinical information from The Cancer Genome Atlas (TCGA) database to identify subtypes of AML associated with lactate metabolism. Two different subtypes linked to lactate metabolism, each with specific immunological features and consequences for prognosis, were identified in this study. Using the TCGA and International Cancer Genome Consortium (GEO) cohorts, a prognostic model composed of genes (LMNA, RETN and HK1) for the prognostic value of the lactate metabolism-related risk score prognostic model was created and validated, suggesting possible therapeutic uses. Additionally, the diagnostic value of the prognostic model genes was explored. LMNA and HK1 were ultimately identified as hub genes, and their roles in AML were determined through immune infiltration, GeneMANIA, GSEA, methylation analysis and single-cell analysis. LMNA was upregulated in AML associating with a poor prognosis while HK1 was downregulated in AML associating with a favorable prognosis. The findings underscore the noteworthy impact of genes linked to lactate metabolism in AML and illustrate the possible therapeutic usefulness of the lactate metabolism-related risk score and the hub lactate metabolism-related genes in guiding AML patients' treatment choices.

Keywords Acute myeloid leukemia, Lactate metabolism-associated gene, OS, Immune signature, Risk model

Acute myeloid leukemia (AML) is a heterogeneous malignancy driven by the accumulation of distinct genetic and epigenetic abnormalities. With the continuous development of conventional chemotherapy, the outcomes of AML patients have significantly improved¹. However, approximately 25% of newly diagnosed AMLs are classified as primary refractory AML. In addition, approximately 70% of the patients who initially achieve CR will eventually relapse. Although extensive efforts have been made to develop salvage chemotherapy, targeted treatment, hematopoietic stem cell transplantation and/or combined therapy, the 5-year survival rate of these patients is only 10%². Therefore, it is important to identify the underlying molecular mechanisms and potential therapeutic targets in AML.

Otto Warburg demonstrated that most cancer cells are highly dependent on aerobic glycolysis³. In AML, many studies have shown that AML blast cells have a unique metabolic signature with increased glycolysis and a correlation with resistance to chemotherapy^{4,5}. As a glucose analog, the glycolysis inhibitor 2-deoxyglucose (2-DG) showed antileukemic activity in both AML cell lines and primary human AML cells^{6,7}. The efficacy and tolerability of 2-DG alone and in combination with other chemotherapeutic agents have also been demonstrated in phase I trials in solid tumors⁸. However, the prognostic role of increased glycolysis remains unclear. By comparing the metabolomic profiles of peripheral blood samples from nearly 400 AML patients with those from 446 healthy controls, Chen et al. generated an AML prognostic risk score and found that increased glycolysis may be associated with poor survival⁴. In contrast, increased glycolysis in AML blast cells from patients at the time of diagnosis was predictive of a better response to therapy and longer survival⁵. A better understanding of glycolysis mechanisms and improved prognostic risk models will allow earlier identification of patients with poor prognosis and personalized treatment strategies.

¹Department of Hematology, Guangdong Provincial Key Laboratory of Major Obstetric Diseases, Guangdong Provincial Clinical Research Center for Obstetrics and Gynecology, The Third Affiliated Hospital, Guangzhou Medical University, Guangzhou, China. ²Department of Clinical Medicine, Guangzhou Medical University, Guangzhou, China. ✉email: lzo19880306@126.com

During glycolysis, cancer cells receive excess glucose and convert it to pyruvate via glycolysis to pyruvate, much of which is then fermented to lactate. The large amounts of lactate and protons secreted by cancer cells or stromal cells play a vital role in the preservation of acidic conditions and promote tumor progression by remodeling the tumor microenvironment (TME), including cell proliferation, angiogenesis, antiapoptotic effects, metastasis and escape from immune surveillance⁹. Extracellular lactate can be sensed by several cell types in the TME, such as T cells, NK cells, dendritic cells and macrophages, and influences their functions. In acidic environments, the antitumor immune response of CD8+ T cells is suppressed, resulting in reduced cytolytic activity and cytokine production. Moreover, extracellular acidosis also suppresses the antitumoral effect of NK cells⁹. To date, various lactate blockade strategies have been explored, such as blocking lactate production and function by targeting LDHA, LDHB, MCT1, MCT4, MCT/CD147, ERK, STAT2, mTOR and other pathways¹⁰.

However, the above relevant studies based on a single gene or key protein in a particular pathway are not effective in predicting the effectiveness of immunosuppressive therapy in patients with AML. In this study, two subtypes associated with lactate metabolism based on the TCGA cohort were identified through an unsupervised clustering algorithm. Differentially expressed genes (DEGs), functional enrichment analysis, and analysis of the tumor microenvironment were applied to determine the differences between the two subtypes. A lactate metabolism-related risk score prognostic model was built through protein and protein interaction (PPI) analysis and the least absolute shrinkage and selection operator (LASSO) Cox regression algorithm, and its potential diagnostic value was also explored. Hub genes were further detected from the prognostic model genes. The underlying mechanism involved immune infiltration, GeneMANIA, GSEA, methylation analysis and single-cell analysis. This provides a new direction for future AML treatment.

Methods

Data collection and tumor somatic mutation analysis

In total, 285 lactate metabolism-associated genes (LMAGs) were identified from the GeneCards database (<https://www.genecards.org/>). For acute myeloid leukemia (AML), the Cancer Genome Atlas (TCGA) and the Gene Expression Omnibus (GEO) were used to retrieve gene expression profiles and related clinical data. Using the GSE9476 dataset, GEO2R software was used to identify genes that were differentially expressed between the AML group and the normal group, with a fold change of 1 and a P value ≤ 0.05 . Clinical prognostic correlation analysis was performed using the TCGA dataset, and prognostic model validation was performed using GSE71014. The GSE116256 dataset was utilized for single-cell analysis, and the GSE90062 dataset was used to validate the expression of the hub genes. All of the above data were obtained from bone marrow samples. Besides, blood samples in GSE9476 dataset were applied to explore the diagnostic value of the constructed prognostic model. In addition, the ggplot2 package was applied to demonstrate the differential expression of DEGs. The “maftool” package was used to analyze the mutational landscape of LMAGs in all TCGA-LAML patients. CNV analysis was carried out on the Gene Set Cancer Analysis (GSCA) website.

Consensus clustering analysis

Consensus Clustering can help researchers identify more robust clustering patterns, and it was utilized to identify lactate metabolism-related subgroups in LAML. According to the expression of LMAGs, patients in TCGA-AML cohort were classified into discrete molecular clusters employing the R packages ‘ConsensusClusterPlus’¹¹, in which ‘hc’ was the method and Pearson was the clustering distance. To ensure the credibility of the classification results, we selected results that were repeated 1000 times. PCA was utilized to display the differences among the subtypes. To detect the DEGs between groups, the “limma” package was applied with the cutoff values set at $|\log_{2}FC| > 1$ and p value < 0.05 . To compare the overall survival of patients in different clusters in the TCGA datasets, Kaplan–Meier survival analysis was used. We also compared the tumor mutation burden (TMB) between the two subtypes. $P \leq 0.05$ was considered to indicate statistical significance.

Functional enrichment analysis and immune landscape of the two LMAGs subtypes

Gene Ontology (GO), Kyoto Encyclopedia of Genes and Genomes (KEGG) and gene set enrichment analysis (GSEA) were used for functional enrichment analysis via the “clusterProfiler” package. The infiltration levels of 22 immune cells in the two subtypes were determined via the “CIBERSORT” package. The “ESTIMATE” package was used to calculate the TME scores (stromal, immune, and ESTIMATE scores) of the samples. In addition, we applied ssGSEA, xCell, MCPcounter, and QuanTIseq algorithm analysis to ensure the reliability of the results. To determine the immune characteristics of the LMAG subtypes, variance analysis of immune checkpoint genes, human leukocyte antigens, and T-cell stimulators were performed.

Construction and validation of the prognostic risk score model and its diagnostic value

To construct the prognostic risk score model, the genes intersecting the LMAGs and DEGs of AML patients were included in the analysis. Protein and protein interaction (PPI) analysis and the least absolute shrinkage and selection operator (LASSO) Cox regression algorithm with 10-fold cross-validation were employed to select genes with pivotal prognostic value. The TCGA cohort was used as the training set, while the GSE71014 cohort was used for validation. The risk score was calculated as follows: Risk score = \sum Coefficient of (i) * expression of gene (i). The “survminer” package was then used to compare OS in different subgroups using the Kaplan–Meier method and Cox regression. We performed univariate and multivariate analyses of model genes, and $P < 0.075$ was considered to indicate statistical significance. The decision curve analysis (DCA) was applied for evaluating the clinical practicality of the final prognostic model. Age, sex, and leukocyte count were incorporated as parameters, and forecasting curves of the nomogram-predicted probability of actual 1-, 3-, and 5-year OS were plotted through the “survival” package and the “rms” package. We analyzed the diagnostic value of the model

genes in both bone marrow samples and blood samples from the GSE9476 dataset using the pROC package and constructed corresponding diagnostic models. An $AUC > 0.7$ was used as a criterion for diagnostic markers.

Exploring potential mechanisms of hub LMAGs in AML

The results of the intersection of key module genes screened before and the DEGs of the two LMAG subtypes were considered the hub LMAGs in AML. The GSE90062 dataset was used for verification. The ssGSEA algorithm was used for immunoinfiltration analysis. The GeneMANIA database was used (<http://genemania.org/>) to investigate the interactions between the hub genes and their associated genes and the involved biological functions. GSCA was used for methylation and CNV analysis. The Tumor Immune Single-cell Hub 2 (TISCH2) website was utilized for analysis of the tumor microenvironment. Moreover, we obtained immunohistochemistry (IHC) images of proteins from bone marrow and gene expression levels of immune cell types based on the HPA database from the Human Protein Atlas (<https://www.proteinatlas.org/>).

Results

Screening of DEGs in AML and the landscape of genetic variation

DEGs of AML were first identified according to the screening criteria p value < 0.05 and $\log|FC| > 1$ from the GSE9476 dataset, which included 470 upregulated and 1139 downregulated genes (Fig. 1A). The expression of the 44 DEGs in each sample is shown in Fig. 1B. Approximately 17.56% of patients had mutations in LMAGs. Figure 1C shows the LMAGs with the highest mutation frequency, and the frequency of DNA mutations in LMAGs ranged from 1 to 7%. Figure 1D,E show the top 10 genes with mutations caused by amplification, among which CBS, SLC19A1, HLCS, MYC, GPT and CYP7A1 were significant in both homozygotes and heterozygotes. Patients with a high TMB frequency had a poorer prognosis than those with a low TMB frequency ($P = 0.088$) (Fig. 1F).

Prognostic analysis and functional enrichment analysis of LMAG-based subtypes

Based on 285 LMAGs, AML patients from the TCGA were divided into two groups (Fig. 2A). A PCA plot showing the difference between the two groups of samples is shown in Fig. 2B. The survival probability was greater in Group 1 than in Group 2 (Fig. 2C). The TMB frequency was greater in Group 2 than in Group 1 ($P < 0.001$) (Fig. 2D). The functional enrichment showed that Group 1 was mainly enriched in the regulation of immune effector process, immune receptor activity, pattern recognition receptor signaling pathway, and immunoregulatory interactions between a lymphoid and a non lymphoid cell and chemokine signaling pathway (Fig. 2E,G). The main enrichment pathways of Group 2 were “cellular response to biotic stimulus”, “osteoclast

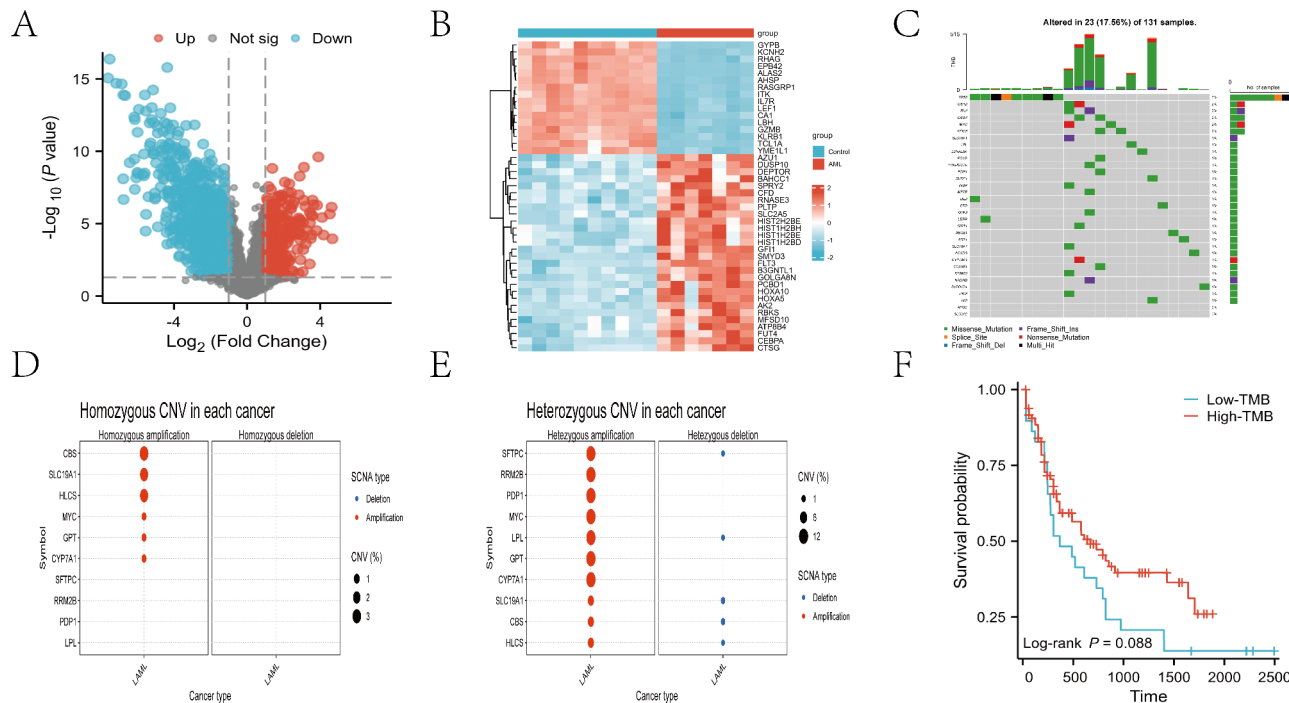


Fig. 1. Differentially expressed genes in AML and analysis of gene mutations related to lactic acid metabolism. (A) Volcano map showing the differentially expressed genes between AML bone marrow samples and control samples. (B) Heatmap of the top 44 differentially expressed genes in the GSE9476 dataset. (C) Lactate metabolism-associated genes alteration frequency in AML patients in TCGA. (D,E) The top ten genes with CNA type as amplification. (F) Overall survival of AML patients in the high-TMB and low-TMB groups. CNA copy number alteration, SCNA somatic copy number alterations, CNV copy number variations, TMB tumor mutation burden.

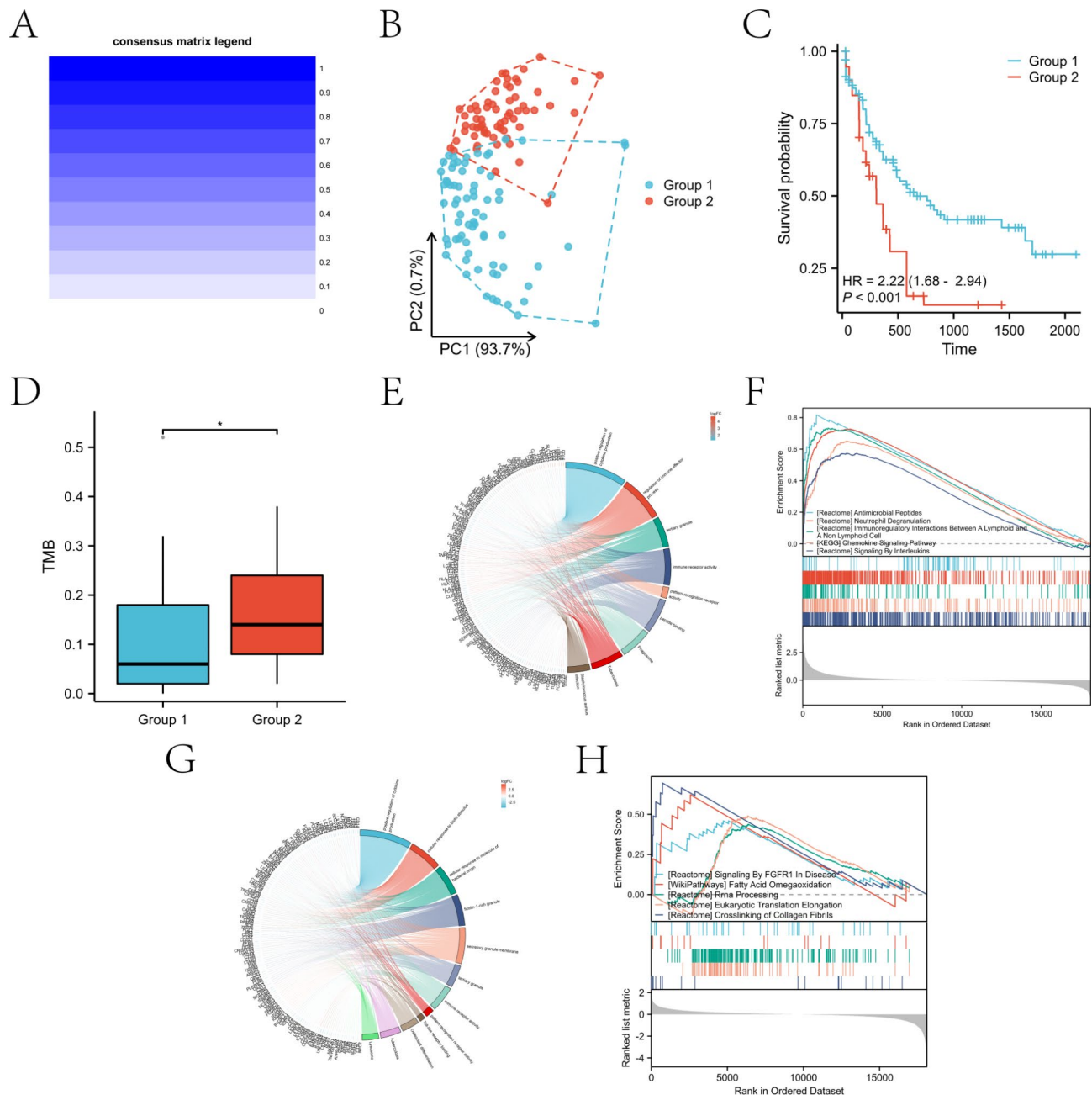


Fig. 2. Consensus clustering of lactate metabolism-associated genes in AML and related functional enrichment analysis. (A) Unsupervised consensus clustering (K-means) was applied to the LAML cohort in TCGA using 1000 iterations for $k=2$, resulting in consensus matrices of patient clusters. (B) Principal component analysis of subtypes in the TCGA cohort. (C) Overall survival of AML patients in group 1 and group 2. (D) Tumor mutation burden frequency between group 1 and group 2. (E) Enriched entries of group 1 obtained from GO and KEGG analyses. (F) Enriched GSEA results for group 1. (G) Enriched entries of group 2 obtained from GO and KEGG analysis. (H) Enriched GSEA results for group 2.

differentiation”, “signaling by FGFR1 in disease” and “crosslinking of collagen fibrils” (Fig. 2F,H). The positive regulation of cytokine production was activated in both Group 1 and Group 2.

Immunocorrelation analysis of subtypes

Immunoinfiltration revealed that naive B cells, plasma cells, CD8 + T cells, resting CD4 + memory T cells, resting NK cells and resting mast cells exhibited high infiltration in Group 2, and Group 1 exhibited high infiltration of monocytes (Fig. 3A; Supplementary Fig. 2). Compared with Group 1, Group 2 had lower stromal, immune, and ESTIMATE scores (Mann-Whitney U test, $P < 0.05$) (Fig. 3B). T-cell stimulators and immune checkpoint genes

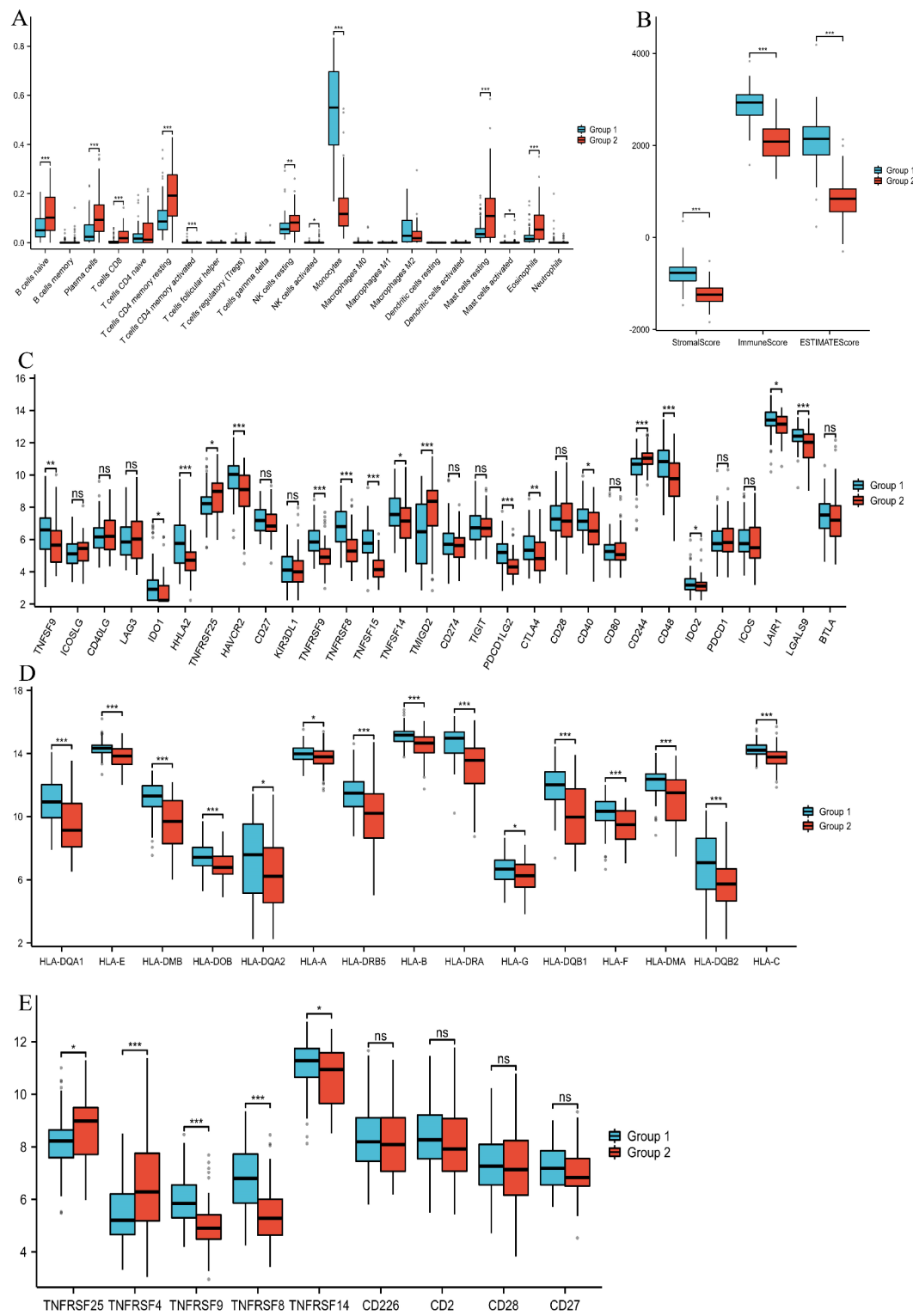


Fig. 3. Immunocorrelation analysis of subtypes. (A) The landscape of immune cell infiltration between the two subtypes. (B) Stromal score, immune score and ESTIMATE score between the two subtypes. (C,D,F) Gene expression of HLA, MHC and immune checkpoint genes in the two clusters.

tended to be more highly expressed in group 1 (Fig. 3C,E). These results imply that the subtypes might react to immunotherapy in distinct ways.

Lactate metabolism-associated prognostic model and diagnostic model

To construct a lactate metabolism-associated prognostic model, we selected 23 genes that were LMAGs among the DEGs of AML patients for further analysis (Fig. 4A). PPIs were constructed for the genes, and 15 genes ordered by degree were identified, which were identified as the top 15 most critical LMAGs in AML (Fig. 4B). Then, LASSO regression was employed to construct a risk score model (Fig. 4C,D). The score calculation formula was as follows: $\text{Riskscore} = (0.0410) * \text{LMNA} + (0.1248) * \text{HK1} + (-0.0341) * \text{RETN}$. The samples were separated into high- and low-risk groups based on the risk score formula (Fig. 4E). OS was significantly greater in the low-risk group ($\text{HR} = 2.61$; $P < 0.001$) (Fig. 4F). The GSE71014 dataset was used for validation of the predictive efficacy of the model, and the model performed well (Fig. 4G,H). We then performed univariate and multivariate analyses of the three genes, and they all showed independent prognostic value (Fig. 4I,J). LMNA and HK1 were risk factors, while RETN was a protective factor. DCA results demonstrated good clinical utility of prognostic modeling (Fig. 4K). We subsequently included age, sex, and WBC count as variables for prognostic calibration analysis, and all three genes exhibited good prognostic value at 1, 3, and 5 years (Fig. 4L), and the nomogram was shown in Fig. 4M. Moreover, we analyzed the diagnostic value of three genes in bone marrow and blood using GSE9476 data. In the bone marrow, the areas under the curve (AUCs) of the ROC curves of LMNA, RETN and HK1 were 0.871, 1 and 1, respectively (Fig. 5A,C). The AUC of the model constructed with the three genes was 1 (Fig. 5D). In the blood samples, the areas under the ROC curves (AUCs) of LMNA, RETN and HK1 were 0.979, 0.716 and 0.789, respectively (Fig. 5F,H). The AUC of the diagnostic model was 0.811 (Fig. 5I). Diagnostic column line graphs of the bone marrow and blood are shown in Fig. 5E,J, respectively. The construction of prognostic models may be able to provide decision support for early diagnosis and treatment in the future. And ROC curve were applied to assess the predictive ability of the diagnostic model.

Identification of the hub LMAG genes of AML and their potential mechanisms in AML

LMNA and HK1 were identified as hub genes because they were also DEGs between the two LMAG-based subtypes (Fig. 6A). The hub genes we screened may serve as future diagnostic markers and therapeutic targets. LMNA expression was upregulated in the GSE90062 and GSE9476 datasets ($P < 0.05$), while HK1 expression was downregulated in both datasets ($P < 0.05$) (Fig. 6B,C). In terms of immune infiltration, the infiltration of macrophages was positively correlated with LMNA expression and significantly differed between the high LMNA expression group and low LMNA expression group ($P < 0.05$) (Fig. 6D,E). The infiltration of macrophages and neutrophils was positively correlated with HK1 expression, while the infiltration of plasmacytoid dendritic cells (pDCs) was negatively correlated with HK1 expression and was significantly different ($P < 0.05$) (Fig. 6F,G). GeneMANIA analysis revealed interactions between LMNA, HK1 and related genes (Fig. 6H,I). LMNA was mainly involved in processes related to glucose metabolism, the NADH metabolic process and nucleoside diphosphate phosphorylation, while HK1 was mainly involved in the regulation of muscle-related biological processes, autophagy and monosaccharide binding. The GSEA results showed that glycosaminoglycan degradation and neutrophil extracellular trap formation were mainly enriched in the high LMNA expression group (Fig. 6J). In the low HK1 expression group, aminoacyl-tRNA biosynthesis, ascorbate and aldarate metabolism, glycosylphosphatidylinositol (GPI)-anchor biosynthesis and lipoic acid metabolism were the major enrichment pathways (Fig. 6K). According to the methylation analysis, methylation was negatively correlated with HK1 expression but was positively correlated with LMNA expression. Mutations in LMNA and HK1 were predominant in the heterozygous amplification group, and mutations in HK1 were also detected in the heterozygous deletion group (Fig. 6L,M).

Heterozygous variants indicate that CNV occurs on one chromosome, whereas pure variants occur on both chromosomes¹². Variations in heterozygous are common types of sCNAs that are associated with cancer development and progression, and this study facilitates further exploration of the role of genes in AML.

Single-cell transcriptome analyses, immunohistochemical staining and expression levels of the hub LMAG genes in immune cell types

Single-cell analysis was performed using the GSE116256 dataset in the TISCH2 database. Thirteen cell types were identified in the datasets (Fig. 7A). Figure 7B,D shows that LMNA was strongly enriched in malignant cells, macrophages and CD8+ T cells, and HK1 was mainly involved in malignant cells, NK cells and CD4+ T cells. THPA was applied to validate the expression of the hub genes in human bone marrow tissues and immune cells. In normal bone marrow, immunohistochemical results revealed low LMNA expression and moderate HK1 expression (Supplementary Fig. 1). In terms of gene expression in various immune cells according to the HPA database, HK1 was highly expressed mainly in macrophages, and its low expression was related to pDCs, while LMNA was highly expressed in T cells (Fig. 7E,F).

Discussion

Since 2010, the first edition of the European Leukemia Network (ELN) has published recommendations for the diagnosis and treatment of AML in adults¹³. In 2017, the ELN was updated for the first time, and risk stratification for AML has been widely used in clinical practice for the diagnosis and risk assessment of AML¹⁴. The recently updated ELN 2022 recommendations revise the genetic risk classification to better categorize those patients whose ELN 2017 classification is unclear, allowing for better differentiation of OS differences between intermediate and poor prognosis groups¹⁵. However, the prognostic significance of ELN 2022 for patients receiving non-intensive therapy and for patients in the adverse risk group for a single myelodysplasia-related mutation is unclear. In addition, the current AML risk stratification system does not predict the patients' response

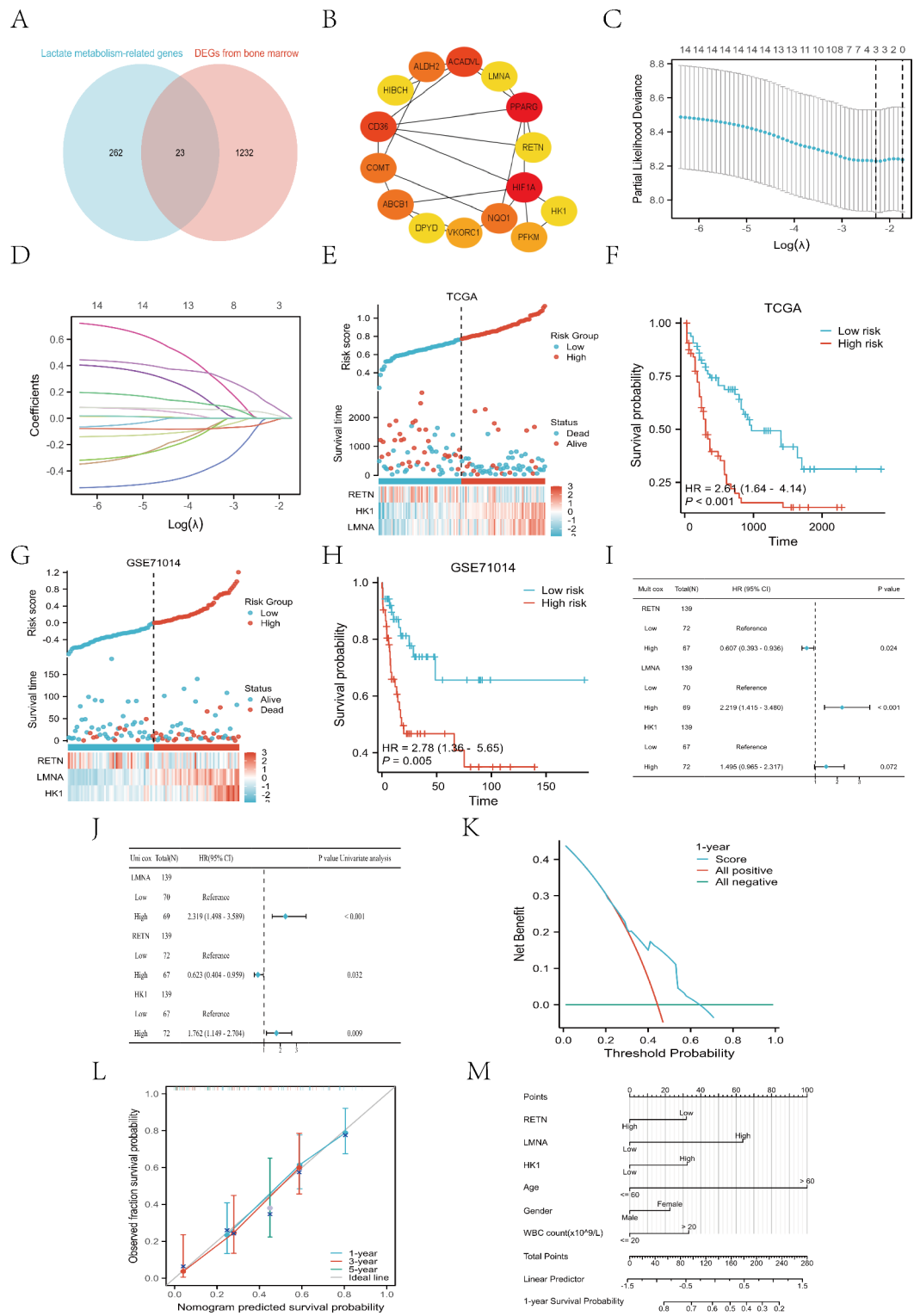


Fig. 4. Development and validation of the lactic acid metabolism-related prognostic models. **(A)** Intersection of DEGs of AML and lactate metabolism-associated genes. **(B)** Protein and protein interaction network of the 15 genes with the highest degrees. **(C,D)** The coefficient distribution of LASSO Cox regression analysis and adjustment parameters were calculated based on partial likelihood deviation and tenfold cross-validation. **(E)** The risk curve, survival status, and model gene expression levels of AML patients in different risk groups in the TCGA cohort. **(F)** Survival analysis between risk groups in the TCGA cohort. **(G)** The risk curve, survival status, and model gene expression levels of AML patients in different risk groups in GSE71014 dataset. **(H)** Survival analysis between risk groups in the GSE71014 dataset. **(I,J)** Univariate and multivariate analyses of the prognostic model genes. **(K)** Result of the decision curve analysis. **(L–M)** Prognostic correction curves and nomogram incorporating age, sex, and WBC count as variables.

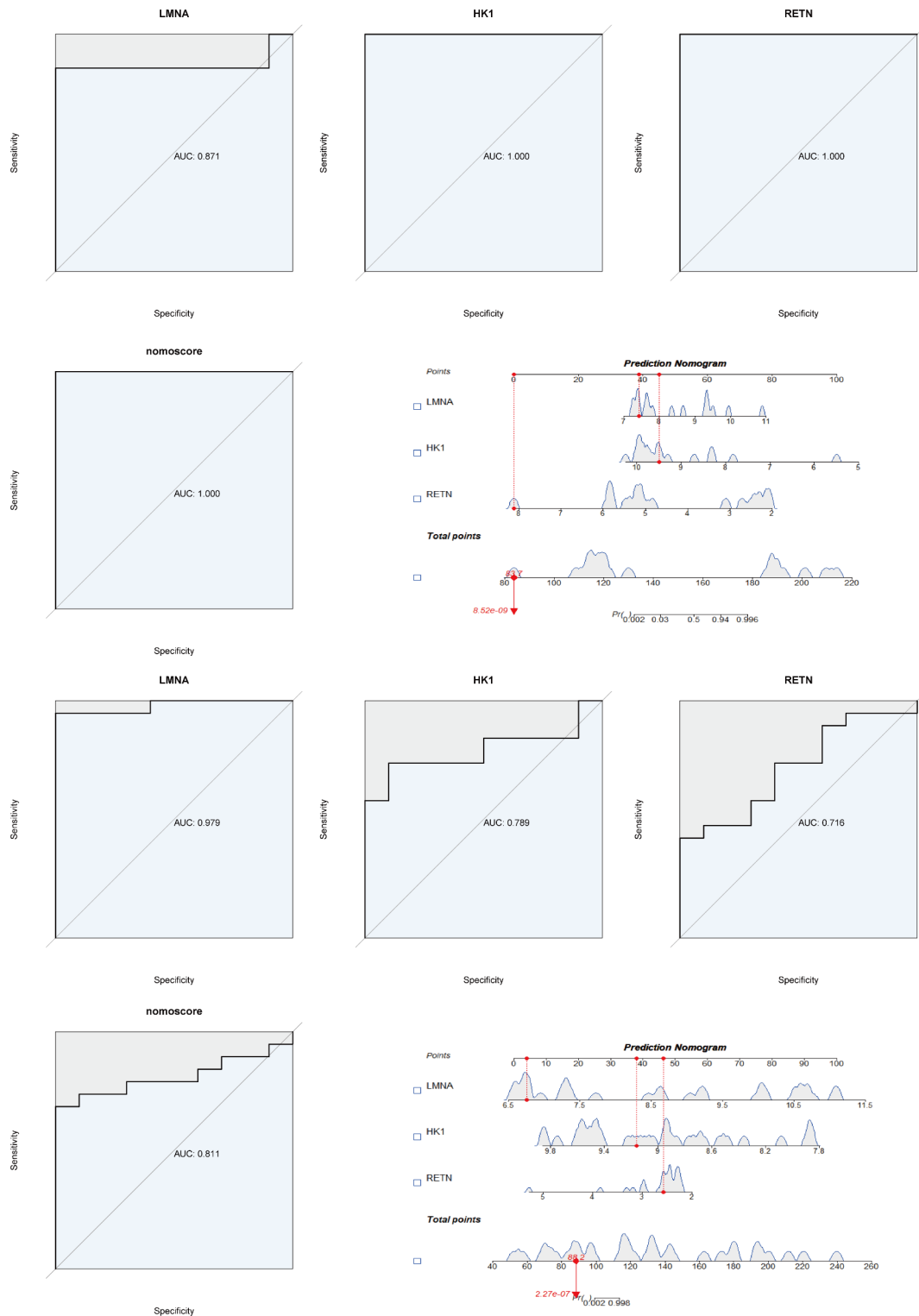


Fig. 5. Development of lactic acid metabolism-related diagnostic models. (A) The ROC curve of LMNA in bone marrow samples in the GSE9476 dataset. (B) The ROC curve of HK1 in bone marrow samples from the GSE9476 dataset. (C) The ROC curve of RETN in bone marrow samples in the GSE9476 dataset. (D) The ROC curve of the model constructed with the three genes in bone marrow samples from the GSE9476 dataset. (E) Diagnostic line chart of bone marrow samples in the GSE9476 dataset. (F) The ROC curve of LMNA in blood samples in the GSE9476 dataset. (G) The ROC curve of HK1 in blood samples in the GSE9476 dataset. (H) The ROC curve of RETN in blood samples in the GSE9476 dataset. (I) The ROC curve of the model constructed with the three genes in blood samples in the GSE9476 dataset. (J) Diagnostic line chart of blood samples in the GSE9476 dataset.

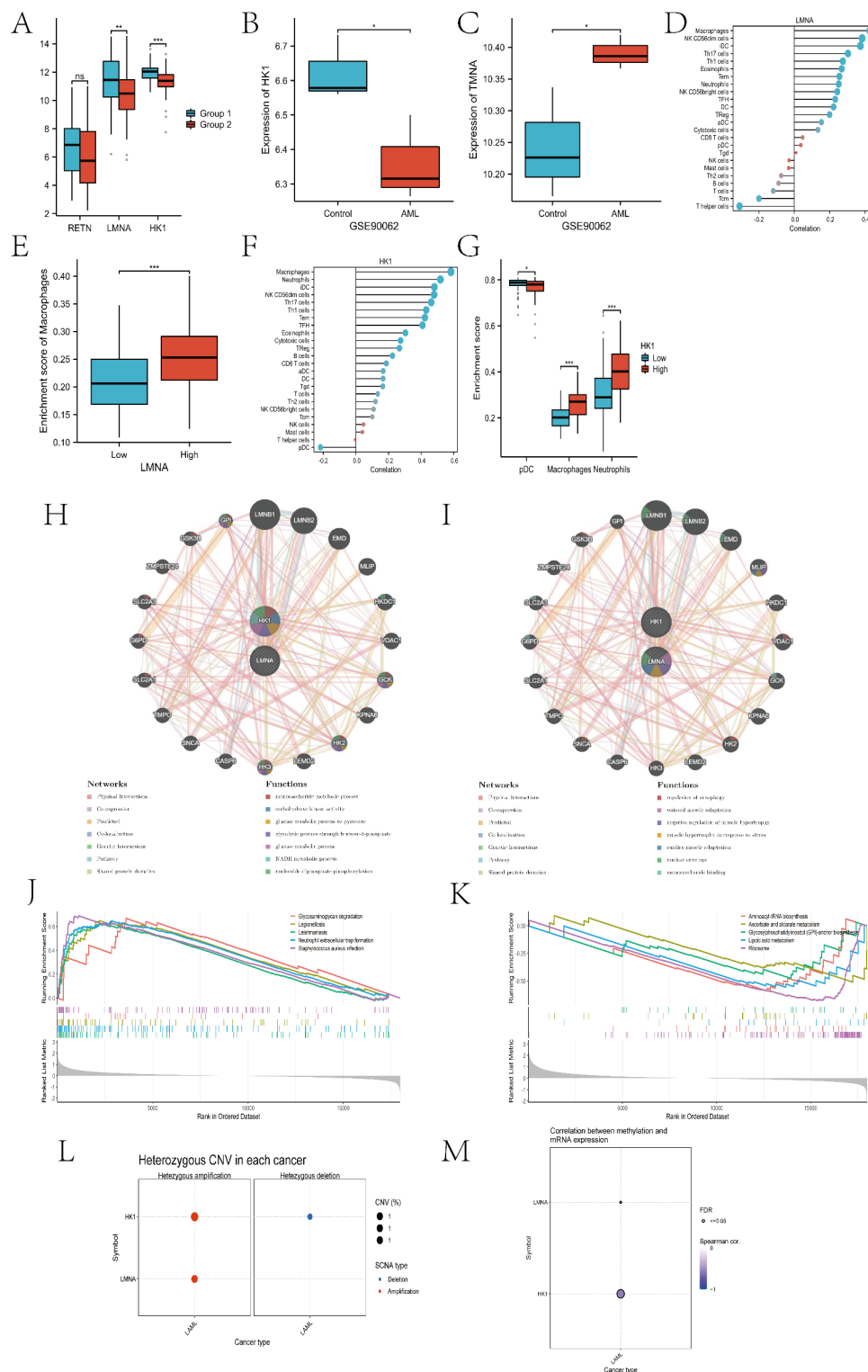


Fig. 6. Hub genes determination and analysis of relevant mechanisms. (A) Lactate metabolism-associated genes that were differentially expressed in both the AML- and LMAG-based subtypes were considered hub genes. (B,C) Validation of the hub genes in GSE90062. (D) Correlation between infiltrating immune cells and the expression of LMNA. (E) Infiltration of macrophages in the high and low LMNA expression groups. (F) Correlation between infiltrating immune cells and the expression of HK1. (G) Infiltration of macrophages, neutrophils and pDCs in the high and low HK1 expression groups. (H,I) Biological processes associated with LMNA, HK1 and their related genes. (J) GSEA results for the AML patients in the high LMNA expression group. (K) GSEA results for the low HK1 expression group in AML. (L) Copy number variation results for LMNA and HK1. (M) Methylation analysis of LMNA and HK1.

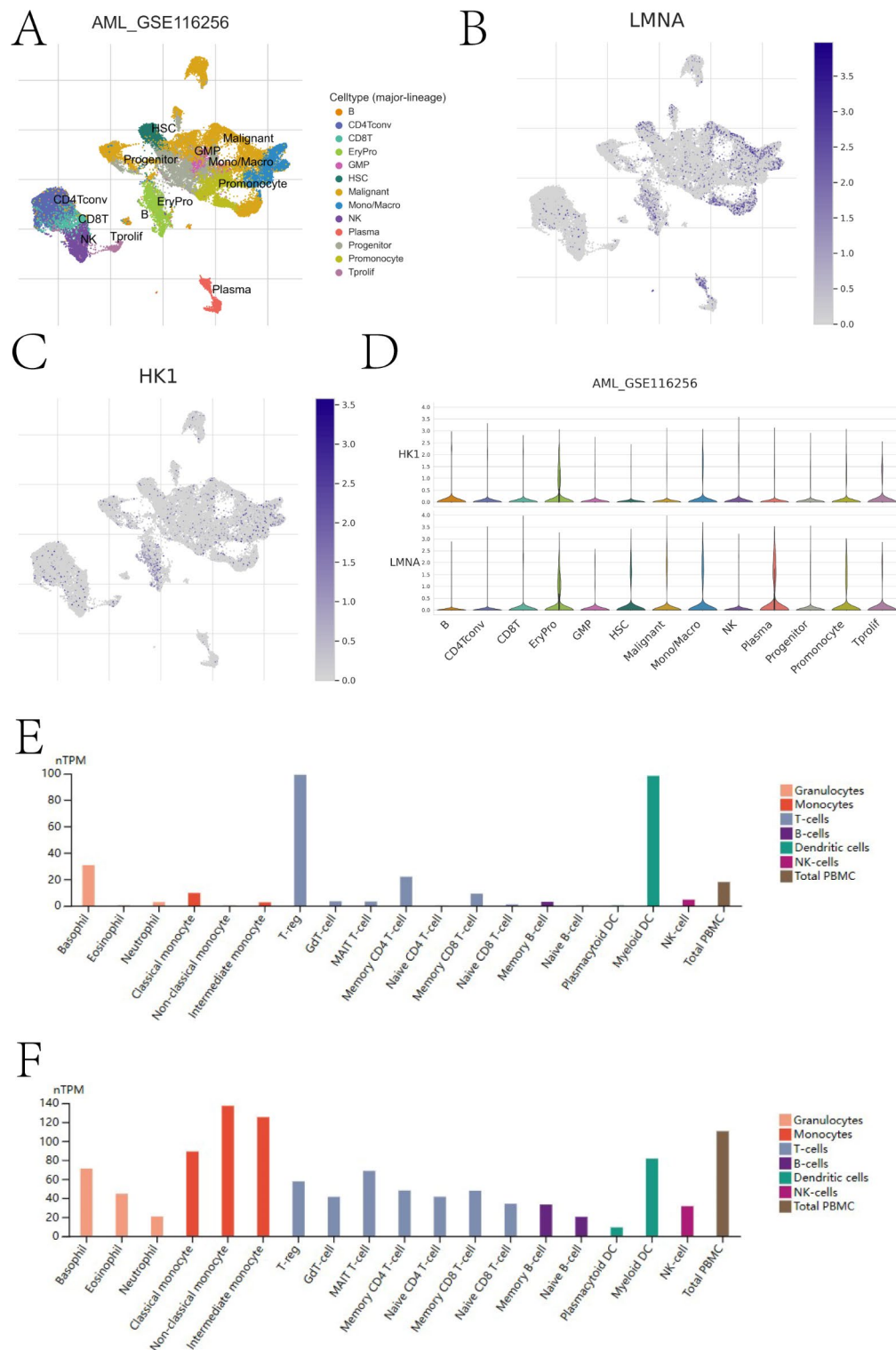


Fig. 7. Single-cell analysis and verification of the hub genes in the Human Protein Atlas (THPA) (A). The identified cell clusters in the AML dataset GSE116256. (B–D) Expression of LMNA and HK1 in various cells. (E) The expression levels of LMNA in immune cell types in the THPA dataset. (F) The expression levels of HK1 in immune cell types in the THPA dataset.

to immunotherapy. Therefore, there is a need to continue to refine methods of prognostic risk assessment for AML and to provide individualized treatment plans for AML patients.

The acid-hostile tumor microenvironment induced by lactic acid accumulation secreted by leukemia cells imposes barriers to tumor-infiltrating immune cells and inhibits durable clinical remission following

immunotherapy. For example, macrophages shift toward the anti-inflammatory subtype (M2 phenotype) to promote cancer progression in leukemia and various types of solid tumors^{16,17}. Moreover, high lactate levels inhibit CD8+ T cell proliferation, cytokine production and cytolytic function¹⁸. In contrast, the immunosuppressive function of regulatory T cells (Treg cells) and myeloid-derived suppressor cells (MDSCs) was maintained, and the expression of programmed death ligand 1 (PD-L1) was also increased on the surface of Treg cells^{19–21}. These findings provide a new perspective on lactic acid-immune crosstalk in the leukemia microenvironment. In this study, a prognostic model based on lactate metabolism in the microenvironment was first established and verified. AML patients from the TCGA database were divided into two groups based on 285 lactate metabolism-related genes identified from the GeneCards database. Survival probability, tumor mutation burden (TMB) frequency, enrichment pathways and immune infiltration characteristics differed between the two groups. Furthermore, a risk score model consisting of the LMNA, HK1 and RETN genes was constructed. AML patients can be divided into high- and low-risk groups based on this risk score model, with patients in the low-risk group having a significantly better OS than those in the high-risk group. Patients in the high-risk group tend to have adaptive immune resistance, which may consist of large numbers of M2-depolarised macrophages and/or activated Treg cells. Treating these patients requires early use of a combined approach—a regimen consisting of chemotherapy, targeted therapy, and intensive immunotherapy. In addition, intermittent fasting, which may recruit CD8+ T cells to tumors by down-regulating the stress-responsive enzyme heme oxygenase-1 and reduce chemotherapy toxicity, is also helpful in treating these patients^{22,23}. We then analyzed the independent prognostic value of each of these three genes and found that LMNA and HK1 could be significant risk factors, while RETN could be considered a protective factor. All three genes showed good prognostic value at 1, 3, and 5 years when age, sex, and WBC count were added as factors for prognostic calibration analysis. The prognostic significance of these three genes has been validated in both peripheral blood and bone marrow samples from patients with AML. The potential clinical application of this prognostic risk model is expected based on its good predictive value and the ease of obtaining test samples.

Lamins are structural components of the nuclear lamina and are critical for maintaining the integrity of the nuclear envelope and cellular morphology²⁴. In cancer cells, the dysregulation of lamins or lamin-related genes, including the lamin A/C (LMNA) leads to altered nuclear structure and morphology²⁵. Reduced LMNA expression is associated with a poor prognosis in patients with gastric cancer²⁶. In contrast, our results showed that LMNA was highly expressed in AML cells and was positively correlated with macrophages, and AML single-cell sequencing confirmed that LMNA was highly expressed in both tumor cells and CD8+ T cells. Regarding CD8+ T-cell function, the frequency of CD8+ T cells expressing checkpoint inhibitory receptors has been demonstrated to increase with disease progression in a mouse model of AML²⁷. Furthermore, a recent phase II clinical trial demonstrated that a high proportion of CD3+ and CD8+ T cells in the bone marrow of AML patients is predictive of the response to a combination of the immune checkpoint inhibitor nivolumab and a demethylating drug²⁸. In light of the aforementioned literature and our findings, we hypothesized that LMNA may play a role in the formation of the AML immune escape microenvironment, involving tumor-associated macrophages and CD8+ T cells. An increase in CD8+ T cells is associated with increased PD-L1 expression in tumor and immune stroma²⁹. This suggests that patients with high LMNA expression may be more suitable for combination therapy with PD-L1 inhibitors.

The family of hexokinases (HKs) catalyzes the first rate-limiting step of the glycolytic pathway, converting glucose to glucose-6-phosphate³⁰. Four isoforms have been identified in mammalian cells, namely, HK1, HK2, HK3 and HK4. It has been reported in the literature that HK1 and HK2 are expressed in a variety of different tissues, with low HK1 and high HK2 expression in tumors, and are involved in the process of tumor initiation, progression and metastasis³¹. Similarly, our results showed that HK1 was expressed at low levels in AML. The infiltration of macrophages and neutrophils was found to be positively correlated with HK1 expression, while the infiltration of pDCs was negatively correlated with HK1 expression. A number of studies have demonstrated that macrophages and neutrophils exhibit considerable heterogeneity and phenotypic plasticity. They are able to detect a variety of mediators present in the tumor microenvironment, which enables them to differentiate into antitumor or protumor phenotypes^{32–34}. Specific tumor-derived factors, such as IL-35, interferon- β (INF- β), and transforming growth factor β (TGF β), or changes in the concentrations of cytokines and oxygen in the tumor microenvironment can influence the switch in the neutrophil phenotype³⁵. Second, these two cell types can also facilitate each other's polarization within the tumor microenvironment³⁶. Consequently, the inhibition of HK1 may disrupt the mutually reinforcing relationship between these two cell types and inhibit immune escape mechanisms in AML. Although HK1 play an important role in promoting immune escape in the leukemia microenvironment, the development of specific inhibitors of HK1 has remained elusive. Because of the effect in repolarizing M2-like tumor-associated macrophages, CD40 agonist antibody³⁷ and TLR9³⁸ agonist could improve the therapeutic efficacy and clinical outcome of AML with high expression of HK1 to a certain extent.

In conclusion, lactate metabolism plays a role in the formation of an immunosuppressive TME in AML by influencing the number and function of multiple immune cells. In our study, a comprehensive analysis of genes related to lactate metabolism in AML was conducted. The findings indicate a strong association between these genes and the predictive value of overall survival and the efficacy of immunosuppressive therapy. However, our research has several limitations. The analysis and establishment of the prognostic model heavily depend on the availability and quality of data from public databases, underscoring the necessity for an expanded sample size. Furthermore, the roles of LMNA, HK1 and RETN in lactate metabolism and immune function within the leukemia microenvironment, as well as the underlying molecular mechanisms, require further validation through *in vitro* and *in vivo* experiments. The assessment of immunotherapy and drug sensitivity in this study necessitates corroboration with clinical data. This exploration will constitute a significant focus of our future research endeavors. The development of therapeutics that target the interplay between lactic acid metabolism

and the immune system in leukemia remains a considerable challenge. A personalized treatment regimen must strike a balance among efficacy, safety and affordability.

Data availability

The data used for bioinformatic analyses were obtained from Gene Expression Omnibus (GEO) at GSE9476, GSE71014, GSE116256 and GSE90062. The data presented in this paper are available by contacting Dr. Zi-yuan Lu via lzo19880306@126.com.

Received: 10 May 2024; Accepted: 17 October 2024

Published online: 28 October 2024

References

1. Pollyea, D. A. et al. Acute myeloid leukemia, Version 3.2023, NCCN Clinical Practice guidelines in Oncology. *J. Natl. Compr. Cancer Netw.* **JNCCN** **21**, 503–513. <https://doi.org/10.6004/jnccn.2023.0025> (2023).
2. DeWolf, S. & Tallman, M. S. How I treat relapsed or refractory AML. *Blood* **136**, 1023–1032. <https://doi.org/10.1182/blood.2019001982> (2020).
3. Mougiaikakos, D. The induction of a permissive environment to promote T cell immune evasion in acute myeloid leukemia: the metabolic perspective. *Front. Oncol.* **9**, 1166. <https://doi.org/10.3389/fonc.2019.01166> (2019).
4. Chen, W. L. et al. A distinct glucose metabolism signature of acute myeloid leukemia with prognostic value. *Blood* **124**, 1645–1654. <https://doi.org/10.1182/blood-2014-02-554204> (2014).
5. Herst, P. M., Howman, R. A., Neeson, P. J., Berridge, M. V. & Ritchie, D. S. The level of glycolytic metabolism in acute myeloid leukemia blasts at diagnosis is prognostic for clinical outcome. *J. Leukoc. Biol.* **89**, 51–55. <https://doi.org/10.1189/jlb.0710417> (2011).
6. Larrue, C. et al. Antileukemic activity of 2-deoxy-D-glucose through inhibition of N-linked glycosylation in acute myeloid leukemia with FLT3-ITD or c-KIT mutations. *Mol. Cancer Ther.* **14**, 2364–2373. <https://doi.org/10.1158/1535-7163.Mct-15-0163> (2015).
7. Grønningseter, I. S. et al. Targeting cellular metabolism in acute myeloid leukemia and the role of patient heterogeneity. *Cells* **9**. <https://doi.org/10.3390/cells9051155> (2020).
8. Raez, L. E. et al. A phase I dose-escalation trial of 2-deoxy-D-glucose alone or combined with docetaxel in patients with advanced solid tumors. *Cancer Chemother. Pharmacol.* **71**, 523–530. <https://doi.org/10.1007/s00280-012-2045-1> (2013).
9. de la Cruz-López, K. G., Castro-Muñoz, L. J., Reyes-Hernández, D. O., García-Carrancá, A. & Manzo-Merino, J. Lactate in the regulation of tumor microenvironment and therapeutic approaches. *Front. Oncol.* **9**, 1143. <https://doi.org/10.3389/fonc.2019.01143> (2019).
10. Byun, J. K. Tumor lactic acid: a potential target for cancer therapy. *Arch. Pharm. Res.* **46**, 90–110. <https://doi.org/10.1007/s12272-023-01431-8> (2023).
11. Wilkerson, M. D. & Hayes, D. N. ConsensusClusterPlus: a class discovery tool with confidence assessments and item tracking. *Bioinformatics* **26**, 1572–1573. <https://doi.org/10.1093/bioinformatics/btq170> (2010).
12. Wang, X. et al. Pan-cancer analysis reveals genomic and clinical characteristics of TRPV channel-related genes. *Front. Oncol.* **12**, 813100. <https://doi.org/10.3389/fonc.2022.813100> (2022).
13. Döhner, H. et al. Diagnosis and management of AML in adults: 2017 ELN recommendations from an international expert panel. *Blood* **129**, 424–447. <https://doi.org/10.1182/blood-2016-08-73196> (2017).
14. Herold, T. et al. Validation and refinement of the revised 2017 European LeukemiaNet genetic risk stratification of acute myeloid leukemia. *Leukemia* **34**, 3161–3172. <https://doi.org/10.1038/s41375-020-0806-0> (2020).
15. Döhner, H. et al. Diagnosis and management of AML in adults: 2022 recommendations from an international expert panel on behalf of the ELN. *Blood* **140**, 1345–1377. <https://doi.org/10.1182/blood.2022016867> (2022).
16. Putthenveetil, A. & Dubey, S. Metabolic reprogramming of tumor-associated macrophages. *Ann. Transl. Med.* **8**, 1030. <https://doi.org/10.21037/atm-20-2037> (2020).
17. Miller, A. et al. Exploring metabolic configurations of single cells within complex tissue microenvironments. *Cell Metab.* **26**, 788–800. [e786](https://doi.org/10.1016/j.cmet.2017.08.010) (2017).
18. Fischer, K. et al. Inhibitory effect of tumor cell-derived lactic acid on human T cells. *Blood* **109**, 3812–3819. <https://doi.org/10.1182/blood-2006-07-035972> (2007).
19. Angelin, A. et al. Foxp3 reprograms T cell metabolism to function in low-glucose. *High-Lactate Environ. Cell Metab.* **25**, 1282–1293e1287. <https://doi.org/10.1016/j.cmet.2016.12.018> (2017).
20. Watson, M. J. et al. Metabolic support of tumour-infiltrating regulatory T cells by lactic acid. *Nature* **591**, 645–651. <https://doi.org/10.1038/s41586-020-03045-2> (2021).
21. Kumagai, S. et al. Lactic acid promotes PD-1 expression in regulatory T cells in highly glycolytic tumor microenvironments. *Cancer Cell* **40**, 201–218e209. <https://doi.org/10.1016/j.ccr.2022.01.001> (2022).
22. Di Biase, S. et al. Fasting-mimicking Diet reduces HO-1 to promote T cell-mediated tumor cytotoxicity. *Cancer Cell* **30**, 136–146. <https://doi.org/10.1016/j.ccr.2016.06.005> (2016).
23. Michalsen, A. & Li, C. Fasting therapy for treating and preventing disease—current state of evidence. *Fortschende Komplementärmedizin* (2006). **20**, 444–453. <https://doi.org/10.1159/000357765> (2013).
24. Kiel, T., Busch, A., Meyer-Rachner, A. & Hübner, S. Laminopathy-inducing mutations reduce nuclear import of expressed prelamin A. *Int. J. Biochem. Cell Biol.* **53**, 271–280. <https://doi.org/10.1016/j.biocel.2014.05.035> (2014).
25. Kim, H. J., Lee, P. C. W. & Hong, J. H. Overview of cellular homeostasis-associated nuclear envelope lamins and associated input signals. *Front. Cell Dev. Biol.* **11**, 1173514. <https://doi.org/10.3389/fcell.2023.1173514> (2023).
26. Brady, G. F., Kwan, R., Bragazzi Cunha, J., Elenbaas, J. S. & Omary, M. B. Lamins and lamin-associated proteins in gastrointestinal health and disease. *Gastroenterology* **154**, 1602–1619e1601. <https://doi.org/10.1053/j.gastro.2018.03.026> (2018).
27. Knaus, H. A. et al. Signatures of CD8+ T cell dysfunction in AML patients and their reversibility with response to chemotherapy. *JCI Insight* **3**. <https://doi.org/10.1172/jci.insight.120974> (2018).
28. Daver, N. et al. Efficacy, Safety, and biomarkers of response to azacitidine and nivolumab in relapsed/refractory acute myeloid leukemia: a nonrandomized, open-label, phase II study. *Cancer Discov.* **9**, 370–383. <https://doi.org/10.1158/2159-8290.Cd-18-0774> (2019).
29. Donizy, P. et al. Prognostic role of tumoral PD-L1 and IDO1 expression, and Intratumoral CD8+ and FoxP3+ lymphocyte infiltrates in 132 primary cutaneous Merkel cell carcinomas. *Int. J. Mol. Sci.* **22**. <https://doi.org/10.3390/ijms2115489> (2021).
30. Seiler, K. et al. Hexokinase 3 enhances myeloid cell survival via non-glycolytic functions. *Cell Death Dis.* **13**, 448. <https://doi.org/10.1038/s41419-022-04891-w> (2022).
31. Patra, K. C. et al. Hexokinase 2 is required for tumor initiation and maintenance and its systemic deletion is therapeutic in mouse models of cancer. *Cancer Cell* **24**, 213–228. <https://doi.org/10.1016/j.ccr.2013.06.014> (2013).

32. Scapini, P. & Cassatella, M. A. Social networking of human neutrophils within the immune system. *Blood* **124**, 710–719. <https://doi.org/10.1182/blood-2014-03-453217> (2014).
33. Hou, P. et al. Macrophage polarization and metabolism in atherosclerosis. *Cell Death Dis.* **14**. <https://doi.org/10.1038/s41419-023-06206-z> (2023).
34. Silvestre-Roig, C., Fridlender, Z. G., Glogauer, M. & Scapini, P. Neutrophil diversity in health and disease. *Trends Immunol.* **40**, 565–583. <https://doi.org/10.1016/j.it.2019.04.012> (2019).
35. Chan, Y. T. et al. Pancreatic melatonin enhances anti-tumor immunity in pancreatic adenocarcinoma through regulating tumor-associated neutrophils infiltration and NETosis. *Acta Pharm. Sin. B* **13**, 1554–1567. <https://doi.org/10.1016/j.apsb.2023.01.020> (2023).
36. Braza, M. S. et al. Neutrophil derived CSF1 induces macrophage polarization and promotes transplantation tolerance. *Am. J. Transplant.* **18**, 1247–1255. <https://doi.org/10.1111/ajt.14645> (2018).
37. Beatty, G. L. et al. CD40 agonists alter tumor stroma and show efficacy against pancreatic carcinoma in mice and humans. *Science (New York N Y)* **331**, 1612–1616. <https://doi.org/10.1126/science.1198443> (2011).
38. Buhtoiarov, I. N. et al. Anti-tumour synergy of cytotoxic chemotherapy and anti-CD40 plus CpG-ODN immunotherapy through repolarization of tumour-associated macrophages. *Immunology* **132**, 226–239. <https://doi.org/10.1111/j.1365-2567.2010.03357.x> (2011).

Author contributions

Ze-min Huang: Conceptualization; Data curation; Formal analysis; Methodology; Project administration; Writing—original draft, Writing—review and editing. Jing Wei: Data curation; Formal analysis; Writing—review and editing. Xiao-wen Pan: Methodology; Formal analysis; Writing—review and editing. Xing-biao Chen: Data curation; Formal analysis; Writing—review and editing. Zi-yuan Lu: Conceptualization; Data curation; Formal analysis; Methodology; Project administration; Writing—original draft, Writing—review and editing.

Funding

This work was supported by the Guangdong Basic and Applied Basic Research Foundation (project no. 2019A1515010390) and the Elite Project Fund of The Third Affiliate Hospital of Guangzhou Medical University (2018001).

Declarations

Competing interests

The authors declare no competing interests.

Additional information

Supplementary Information The online version contains supplementary material available at <https://doi.org/10.1038/s41598-024-76919-4>.

Correspondence and requests for materials should be addressed to Z.-y.L.

Reprints and permissions information is available at www.nature.com/reprints.

Publisher's note Springer Nature remains neutral with regard to jurisdictional claims in published maps and institutional affiliations.

Open Access This article is licensed under a Creative Commons Attribution-NonCommercial-NoDerivatives 4.0 International License, which permits any non-commercial use, sharing, distribution and reproduction in any medium or format, as long as you give appropriate credit to the original author(s) and the source, provide a link to the Creative Commons licence, and indicate if you modified the licensed material. You do not have permission under this licence to share adapted material derived from this article or parts of it. The images or other third party material in this article are included in the article's Creative Commons licence, unless indicated otherwise in a credit line to the material. If material is not included in the article's Creative Commons licence and your intended use is not permitted by statutory regulation or exceeds the permitted use, you will need to obtain permission directly from the copyright holder. To view a copy of this licence, visit <http://creativecommons.org/licenses/by-nc-nd/4.0/>.

© The Author(s) 2024